Proceedings of 7th International Symposium on Cavitation
CAV2009 – Paper No.#7
August 16–20, 2009, Ann Arbor, Michigan, USA

WEAKLY NONLINEAR ANALYSIS OF DISPERSIVE WAVES IN MIXTURES OF LIQUID AND GAS BUBBLES BASED ON A TWO-FLUID MODEL

Tetsuya KANAGAWA
Division of Mechanical and Space Engineering
Hokkaido University
Sapporo, 060–8628, Japan
Email: kanagawa@mech-me.eng.hokudai.ac.jp

Takeru YANO
Division of Mechanical Engineering
Osaka University
Suita, 565–0871, Japan
Email: yano@mech.eng.osaka-u.ac.jp

Masao WATANABE
Division of Mechanical and Space Engineering
Hokkaido University
Sapporo, 060–8628, Japan
Email: masao.watanabe@eng.hokudai.ac.jp

Shigeo FUJIKAWA
Division of Mechanical and Space Engineering
Hokkaido University
Sapporo, 060–8628, Japan
Email: fujikawa@eng.hokudai.ac.jp

ABSTRACT

One-dimensional nonlinear dispersive waves in liquids containing a number of microbubbles are theoretically studied based on two-fluid averaged equations derived by the present authors. The set of equations consists of the conservation laws of mass and momentum for gas and liquid phases, and the equation of motion of the bubble wall. The compressibility of liquid is taken into account, and this leads to the wave attenuation due to bubble oscillations. By using the method of multiple scales, two types of equations for nonlinear wave propagation in long ranges are derived. In a moderately low frequency band, the behavior of weakly nonlinear waves is described by the Korteweg–de Vries–Burgers equation. On the other hand, in a moderately high frequency band, the nonlinear modulation of quasi-monochromatic wave train is described by the nonlinear Schrödinger equation with an attenuation term.

INTRODUCTION

The characteristics of sound waves in bubbly liquids are considerably different from those in single phase fluids [1–10]. Especially, the dispersion in the sense that waves of different wavelengths propagate with different phase velocities is an important property, which is caused by bubble oscillations.

Egashira *et al.* [11] have derived a set of averaged equations based on a two-fluid model. On the basis of these equations, we have analyzed one-dimensional linear dispersive waves in bubbly liquids [11–13]. By considering the compressibility of the liquid phase, we have shown the existence of the two propagation modes of pressure waves, i.e., slow mode and fast mode.

In the present paper, we shall extend the previous studies [11–13] to nonlinear wave motions. The one-dimensional nonlinear dispersive waves in liquids containing a number of small spherical gas bubbles of slow mode are theoretically investigated. The compressibility of the liquid phase is taken into account in the same way as the previous studies, and this leads to an attenuation effect due to acoustic radiation caused by bubble oscillations.

Figure 1 shows the linear dispersion relation of slow mode [11]. Here, Band A and Band B in Fig. 1 correspond to the moderately low and high frequency bands, and these are regarded as the weakly and strongly dispersive bands, respectively. We

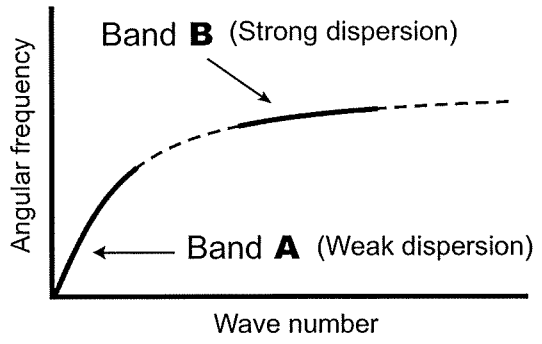

Figure 1. The dispersion relation of the slow mode in a bubbly quiescent liquid [11]. Band A and Band B correspond to the weakly and strongly dispersive bands, respectively.

shall prescribe both Band A and Band B by an appropriate scaling of parameters. The weakly nonlinear propagations of pressure waves in both Band A and Band B are studied by the use of the method of multiple scales. As a result, the behaviors of waves in Band A and Band B are described by the Korteweg–de Vries–Burgers equation [3, 14] and the nonlinear Schrödinger equation [5, 14] with an attenuation term, respectively.

In this paper, we shall demonstrate that appropriate scalings of a set of physical parameters enable us to do systematic derivations of the Korteweg–de Vries–Burgers equation and the nonlinear Schrödinger equation from a set of basic equations for bubbly flows.

FORMULATION OF THE PROBLEM

We shall analyze one-dimensional nonlinear dispersive waves in mixtures of a liquid and a number of small spherical gas bubbles on the basis of the averaged equations. At an initial state, the mixtures are assumed to be uniform and at rest. The pressure waves are generated by oscillations of a sound source in the bubbly liquid.

The compressibility of liquid phase is taken into account. For the simplicity, we neglect the viscosity of gas phase, the thermal conductivity of gas and liquid phases, the phase change across the gas-liquid interface, and the Reynolds stress.

Governing equations

The system of governing equations of bubbly flows is composed of the mass and momentum conservation laws, the equation of motion for the bubble wall, the equations of state for gas and liquid, and so on [11–13]. For the one-dimensional waves, the conservation laws of the mass and momentum for gas and liquid phases based on a two-fluid model by Egashira *et al.* [11] are written as follows:

$$\frac{\partial}{\partial t^*}(\alpha\rho_G^*)+\frac{\partial}{\partial x^*}(\alpha\rho_G^* u_G^*)=0, \tag{1}$$

$$\frac{\partial}{\partial t^*}[(1-\alpha)\rho_L^*]+\frac{\partial}{\partial x^*}[(1-\alpha)\rho_L^* u_L^*]=0, \tag{2}$$

$$\frac{\partial}{\partial t^*}(\alpha\rho_G^* u_G^*)+\frac{\partial}{\partial x^*}\left(\alpha\rho_G^* {u_G^*}^2\right)+\alpha\frac{\partial p_G^*}{\partial x^*}=F^*, \tag{3}$$

$$\frac{\partial}{\partial t^*}[(1-\alpha)\rho_L^* u_L^*]+\frac{\partial}{\partial x^*}\left[(1-\alpha)\rho_L^* {u_L^*}^2\right] +(1-\alpha)\frac{\partial p_L^*}{\partial x^*}+P^*\frac{\partial\alpha}{\partial x^*}=-F^*, \tag{4}$$

where t^* is the time, x^* is the space coordinate normal to the wave front, α is the volume fraction of the gas phase ($0<\alpha<1$), ρ^* is the density, u^* is the fluid velocity, p^* is the pressure, and the subscripts G and L denote volume-averaged variables in gas and liquid phases, respectively. In addition to the volume-averaged pressures p_G^* and p_L^*, P^* is introduced as the liquid pressure averaged on the gas-liquid interface. Here and hereafter, the superscript "$*$" denotes dimensional quantities.

As the interfacial momentum transport F^*, we employ the following model of the virtual mass force [12, 15, 16]

$$F^*=-\beta_1\alpha\rho_L^*\left(\frac{D_G u_G^*}{Dt^*}-\frac{D_L u_L^*}{Dt^*}\right) -\beta_2\rho_L^*(u_G^*-u_L^*)\frac{D_G\alpha}{Dt^*}-\beta_3\alpha(u_G^*-u_L^*)\frac{D_G\rho_L^*}{Dt^*}, \tag{5}$$

where the values of coefficients β_1, β_2, and β_3 may be set as $1/2$. Here, the operators D_G/Dt^* and D_L/Dt^* are defined as

$$\frac{D_G}{Dt^*}\equiv\frac{\partial}{\partial t^*}+u_G^*\frac{\partial}{\partial x^*}, \tag{6}$$

$$\frac{D_L}{Dt^*}\equiv\frac{\partial}{\partial t^*}+u_L^*\frac{\partial}{\partial x^*}. \tag{7}$$

The Keller equation for oscillations of the spherical bubble in the compressible liquid is introduced as follows [17]:

$$\left(1-\frac{1}{c_{L0}^*}\frac{D_G R^*}{Dt^*}\right)R^*\frac{D_G^2 R^*}{Dt^{*2}}+\frac{3}{2}\left(1-\frac{1}{3c_{L0}^*}\frac{D_G R^*}{Dt^*}\right)\left(\frac{D_G R^*}{Dt^*}\right)^2 =\left(1+\frac{1}{c_{L0}^*}\frac{D_G R^*}{Dt^*}\right)\frac{P^*}{\rho_{L0}^*}+\frac{R^*}{\rho_{L0}^* c_{L0}^*}\frac{D_G}{Dt^*}(p_L^*+P^*), \tag{8}$$

where R^* is the bubble radius, c_{L0}^* and ρ_{L0}^* are, respectively, the speed of sound and the density in liquid phase at the initial unperturbed state. The second term in the right-hand side of Eq. (8) is

responsible for the wave attenuation due to the acoustic radiation due to bubble oscillations.

In order to close the system of equations (1)–(5) and (8), the following equations are used: (i) the polytropic equation of state for gas,

$$\frac{p_G^*}{p_{G0}^*} = \left(\frac{\rho_G^*}{\rho_{G0}^*}\right)^{\gamma}, \tag{9}$$

(p_{G0}^* and ρ_{G0}^* are, respectively, the pressure and density inside the bubble in the unperturbed state, and γ is the polytropic exponent), (ii) the Tait equation of state for liquid,

$$p_L^* = p_{L0}^* + \frac{\rho_{L0}^* c_{L0}^{*2}}{n}\left[\left(\frac{\rho_L^*}{\rho_{L0}^*}\right)^n - 1\right], \tag{10}$$

(p_{L0}^* is the liquid pressure in the unperturbed state, and $n = 7.15$ is used if the liquid is water), (iii) the conservation law of mass inside the bubble,

$$\frac{\rho_G^*}{\rho_{G0}^*} = \left(\frac{R_0^*}{R^*}\right)^3, \tag{11}$$

(R_0^* is the bubble radius in the unperturbed state), (iv) the pressure balance at the gas-liquid interface,

$$p_G^* - (p_L^* + P^*) = \frac{2\sigma^*}{R^*} + \frac{4\mu^*}{R^*}\frac{D_G R^*}{Dt^*}, \tag{12}$$

where σ^* is the surface tension, and μ^* is the liquid viscosity. Note that all the variables in the initial unperturbed state, c_{L0}^*, ρ_{L0}^*, ρ_{G0}^*, p_{L0}^*, p_{G0}^*, and R_0^*, are constants.

The liquid viscosity μ^* in Eq. (12) has dropped in Eq. (4). This is because the perturbation of the liquid density is regarded as significantly small compared with that of other variables, although the liquid compressibility is taken into account in the present study. Therefore, we neglect the term of coupling of the liquid viscosity and compressibility in the momentum equation with the assumption of spherical symmetry.

Perturbation expansions

We shall use the method of multiple scales (see, e.g., [14]), to derive the so-called far-field equations, which describe slow variations of behavior in the propagation process of long ranges of weakly nonlinear waves.

Firstly, the time t^* and the space coordinate x^* are, respectively, normalized by

$$t = \frac{t^*}{T^*}, \qquad x = \frac{x^*}{L^*}, \tag{13}$$

where T^* and L^* are the characteristic time and length, respectively. We introduce the new independent variables defined by t, x, and a small nondimensional parameter $\varepsilon\,(\ll 1)$:

$$t_m = \varepsilon^m t, \quad x_m = \varepsilon^m x \quad (m = 0, 1, 2, \cdots), \tag{14}$$

where $t_0 = t$ and $x_0 = x$ represent fast scales, whereas $t_1 = \varepsilon t$, $x_1 = \varepsilon x$, and so on, represent slow scales, and are called as slow variables. The small parameter ε denotes a typical amplitude of waves. By using chain rules and Eq. (14), the differential operators can be expanded as follows [14]:

$$\frac{\partial}{\partial t} = \frac{\partial}{\partial t_0} + \varepsilon\frac{\partial}{\partial t_1} + \varepsilon^2\frac{\partial}{\partial t_2} + O(\varepsilon^3), \tag{15}$$

$$\frac{\partial}{\partial x} = \frac{\partial}{\partial x_0} + \varepsilon\frac{\partial}{\partial x_1} + \varepsilon^2\frac{\partial}{\partial x_2} + O(\varepsilon^3). \tag{16}$$

The four dependent variables, α, u_G^*, u_L^*, and R^*, are nondimensionalized and expanded in a power series of ε, as follows:

$$\alpha/\alpha_0 = 1 + \varepsilon\alpha_1 + \varepsilon^2\alpha_2 + O(\varepsilon^3), \tag{17}$$

$$u_G^*/U^* = \varepsilon u_{G1} + \varepsilon^2 u_{G2} + O(\varepsilon^3), \tag{18}$$

$$u_L^*/U^* = \varepsilon u_{L1} + \varepsilon^2 u_{L2} + O(\varepsilon^3), \tag{19}$$

$$R^*/R_0^* = 1 + \varepsilon R_1 + \varepsilon^2 R_2 + O(\varepsilon^3), \tag{20}$$

where α_0 is the initial volume fraction and U^* is the characteristic velocity. In Eqs. (17)–(20) and the following equations, all expansion coefficients are of $O(1)$. The characteristic velocity U^* is a typical propagation speed of waves, the characteristic time T^* is a typical period of the incident wave, and the characteristic length $L^* \equiv U^*T^*$ is a typical wavelength.

Furthermore, the expansion of the liquid density ρ_L^* is defined as

$$\rho_L^*/\rho_{L0}^* = 1 + \varepsilon^a\rho_{L1} + \varepsilon^{a+1}\rho_{L2} + O(\varepsilon^{a+2}), \tag{21}$$

where $a\,(>1)$ is an integer number, whose explicit values are to be determined in the following sections, by considering the conditions of each problem. We shall remark that the expansion of the liquid density begins with $O(\varepsilon^a)$ in Eq. (21), which is because the compressibility of liquid is very small compared with that of gas.

Substituting Eq. (21) into the Tait equation (10) gives the expansion of the liquid pressure p_L^* as

$$p_L \equiv \frac{p_L^*}{\rho_{L0}^* U^{*2}} = \frac{p_{L0}^*}{\rho_{L0}^* U^{*2}} + \varepsilon^{a-2b}\frac{\rho_{L1}}{V^2} + \varepsilon^{a-2b+1}\frac{\rho_{L2}}{V^2} + O(\varepsilon^{a-2b+2}), \tag{22}$$

where $V\varepsilon^b$ is introduced as a measure of the ratio of the characteristic velocity and the speed of sound in liquid in the unperturbed state,

$$\frac{U^*}{c^*_{L0}} \equiv V\varepsilon^b \equiv O(\varepsilon^b). \tag{23}$$

The parameter V is of $O(1)$ and b is a real number to be determined. Since the perturbation in the liquid pressure should begin with the $O(\varepsilon)$ term in Eq. (22), as in the expansions (17)–(20), the following condition is required

$$a - 2b = 1. \tag{24}$$

Hence Eq. (22) may be rewritten as

$$p_L = p_{L0} + \varepsilon\frac{p_{L1}}{V^2} + \varepsilon^2\frac{p_{L2}}{V^2} + O(\varepsilon^3). \tag{25}$$

In addition, the nondimensional pressures for gas and liquid in the unperturbed state, p_{G0} and p_{L0}, are introduced as

$$p_{G0} \equiv \frac{p^*_{G0}}{\rho^*_{L0}U^{*2}} \equiv O(1), \qquad p_{L0} \equiv \frac{p^*_{L0}}{\rho^*_{L0}U^{*2}} \equiv O(1), \tag{26}$$

respectively. The ratio of initial densities of gas and liquid is assumed to be of $O(\varepsilon^3)$:

$$\frac{\rho^*_{G0}}{\rho^*_{L0}} \equiv O(\varepsilon^3). \tag{27}$$

The nondimensional liquid viscosity μ is introduced as

$$\mu \equiv \frac{\mu^*}{\varepsilon^2\rho^*_{L0}R^*_0U^*} \equiv O(1). \tag{28}$$

NONLINEAR WAVE OF WEAK DISPERSION

In this section, we shall analyze the weakly nonlinear propagation of pressure waves in the moderately low frequency band, i.e., Band A in Fig. 1. Band A is regarded as the weakly dispersive band.

To characterize the problem, we shall choose the scalings of three parameters, U^*, L^*, and T^*, as follows:

$$\frac{U^*}{c^*_{L0}} \equiv O(\sqrt{\varepsilon}) \equiv V\sqrt{\varepsilon}, \tag{29}$$

$$\frac{R^*_0}{L^*} \equiv O(\sqrt{\varepsilon}) \equiv \Delta\sqrt{\varepsilon}, \tag{30}$$

$$\frac{\omega^*}{\omega^*_B} \equiv \frac{1}{T^*\omega^*_B} \equiv O(\sqrt{\varepsilon}) \equiv \Omega\sqrt{\varepsilon}, \tag{31}$$

where Δ and Ω are constants of $O(1)$ (Ω corresponds to a normalized frequency of waves), $\omega^* \equiv 1/T^*$ is a frequency of the sound source, and ω^*_B is the eigenfrequency of linear spherical symmetric oscillation of single bubble,

$$\omega^*_B \equiv \sqrt{\frac{3\gamma p^*_{G0} - 2\sigma^*/R^*_0}{\rho^*_{L0}R^{*2}_0}}. \tag{32}$$

For the simplicity, the effects of liquid compressibility and viscosity are neglected in Eq. (32), i.e., ω^*_B is the same as the eigenfrequency obtained from the linearized Rayleigh–Plesset equation.

The set of scalings (29)–(31) shows that the focused wave motion is of low frequency compared with the eigenfrequency of bubble, of large wavelength compared with the initial bubble radius, and of small propagation speed compared with the speed of sound in the liquid phase.

Comparison of Eq. (24) with Eq. (29) yields $a = 2$, and hence the expansions of the liquid density (21) and the liquid pressure (25), respectively, may be rewritten as

$$\rho^*_L/\rho^*_{L0} = 1 + \varepsilon^2\rho_{L1} + \varepsilon^3\rho_{L2} + O(\varepsilon^4), \tag{33}$$

$$p_L = p_{L0} + \varepsilon p_{L1} + \varepsilon^2 p_{L2} + O(\varepsilon^3), \tag{34}$$

where the expansion coefficients in Eq. (34) are defined as

$$p_{L1} = \frac{\rho_{L1}}{V^2}, \quad p_{L2} = \frac{\rho_{L2}}{V^2}. \tag{35}$$

The following analysis in this section requires only the slow variables, $t_1 = \varepsilon t$, and therefore Eq. (15) may be simplified into

$$\frac{\partial}{\partial t} = \frac{\partial}{\partial t_0} + \varepsilon\frac{\partial}{\partial t_1}. \tag{36}$$

First-order equations

We substitute expansions (17)–(20), (33) and (34) into basic equations (1)–(4) and (8)–(12), and use scalings (29)–(31), derivative expansion (36), and so on. As a result, we firstly obtain the following set of linearized equations as the first-order equations: the mass conservation law in gas phase,

$$\frac{\partial\alpha_1}{\partial t_0} - 3\frac{\partial R_1}{\partial t_0} + \frac{\partial u_{G1}}{\partial x} = 0, \tag{37}$$

the mass conservation law in liquid phase,

$$\alpha_0\frac{\partial\alpha_1}{\partial t_0} - (1-\alpha_0)\frac{\partial u_{L1}}{\partial x} = 0, \tag{38}$$

the momentum conservation law in gas phase,

$$\beta_1 \frac{\partial u_{G1}}{\partial t_0} - \beta_1 \frac{\partial u_{L1}}{\partial t_0} - 3\gamma p_{G0} \frac{\partial R_1}{\partial x} = 0, \tag{39}$$

the momentum conservation law in liquid phase,

$$(1-\alpha_0+\beta_1\alpha_0)\frac{\partial u_{L1}}{\partial t_0} - \beta_1\alpha_0 \frac{\partial u_{G1}}{\partial t_0} + (1-\alpha_0)\frac{\partial p_{L1}}{\partial x} = 0, \tag{40}$$

and the Keller equation,

$$p_{L1} + \frac{\Delta^2}{\Omega^2} R_1 = 0. \tag{41}$$

Eliminating α_1, u_{G1}, u_{L1}, and p_{L1} from Eqs. (37)–(41), the linear wave equation can be derived as

$$\frac{\partial^2 R_1}{\partial t_0^2} - v_p^2 \frac{\partial^2 R_1}{\partial x^2} = 0, \tag{42}$$

where the phase velocity v_p is

$$v_p = \sqrt{\frac{3\alpha_0(1-\alpha_0+\beta_1)\gamma p_{G0} + \beta_1(1-\alpha_0)\Delta^2/\Omega^2}{3\beta_1\alpha_0(1-\alpha_0)}}. \tag{43}$$

Similarly to the well-known speed of sound in the incompressible liquid containing gas bubbles [2, 3], v_p is in proportion to $1/\sqrt{\alpha_0(1-\alpha_0)}$. This is the reflection of the fact that the expansion of the liquid density starts with $O(\varepsilon^2)$ in Eq. (33), i.e., the compressibility of liquid may be regarded as so weak. Now, we choose the characteristic velocity U^* as

$$U^* = \sqrt{\frac{3\alpha_0(1-\alpha_0+\beta_1)\gamma p^*_{G0}/\rho^*_{L0} + \beta_1(1-\alpha_0)R_0^{*2}\omega_B^{*2}}{3\beta_1\alpha_0(1-\alpha_0)}}, \tag{44}$$

and this leads to $v_p \equiv 1$. Rewriting R_1 into f in Eq. (42), we have

$$\frac{\partial^2 f}{\partial t_0^2} - \frac{\partial^2 f}{\partial x^2} = 0. \tag{45}$$

That is, the near field is described by the linear wave equation (45), and the dispersion and dissipation effects of waves due to bubble oscillations do not appear there.

Second-order equations

Let us derive the second-order equations. By the use of the same procedure as the derivation of Eq. (42), we have

$$\frac{\partial^2 R_2}{\partial t_0^2} - \frac{\partial^2 R_2}{\partial x^2} = H(x, t_0, t_1), \tag{46}$$

where the inhomogeneous term, H, is composed of the partial derivatives of the first-order expansion coefficients (e.g., u_{G1}, R_1) with respect to x, t_0, and t_1.

Focusing on the right-running wave, the phase function $\hat{\varphi}$ is introduced as

$$\hat{\varphi} \equiv x - t_0. \tag{47}$$

Rewriting Eqs. (37)–(41) by $\hat{\varphi}$ and integrating them with respect to $\hat{\varphi}$, we can express α_1, u_{G1}, u_{L1}, and p_{L1}, as multiples of $f = R_1$, and hence the inhomogeneous term H in Eq. (46) may be regarded as a function of $\hat{\varphi}$ and t_1.

The solvability condition or the non-secular condition requires

$$H(\hat{\varphi}, t_1) = 0. \tag{48}$$

From Eq. (48), we can derive a far-field equation

$$\frac{\partial f}{\partial t_1} + C_0 \frac{\partial f}{\partial \hat{\varphi}} + C_1 f \frac{\partial f}{\partial \hat{\varphi}} + C_2 \frac{\partial^2 f}{\partial \hat{\varphi}^2} + C_3 \frac{\partial^3 f}{\partial \hat{\varphi}^3} = 0, \tag{49}$$

where the coefficients of advective, dissipative, and dispersive terms, C_0, C_2, and C_3, are given by

$$C_0 = -\frac{(1-\alpha_0)\Delta^2 V^2}{6\alpha_0\Omega^2}, \tag{50}$$

$$C_2 = -\frac{\Delta^3 V}{6\alpha_0\Omega^2}, \tag{51}$$

$$C_3 = \frac{\Delta^2}{6\alpha_0}, \tag{52}$$

respectively. Clearly, C_0 and C_2 have negative values, while C_3 has a positive value. In the present paper, the explicit representation of the coefficient of the nonlinear term C_1 is not shown because of the complexity of expression.

Introducing a modified phase function φ

$$\varphi \equiv \hat{\varphi} - C_0 t_1 = x - t_0 - C_0 t_1, \tag{53}$$

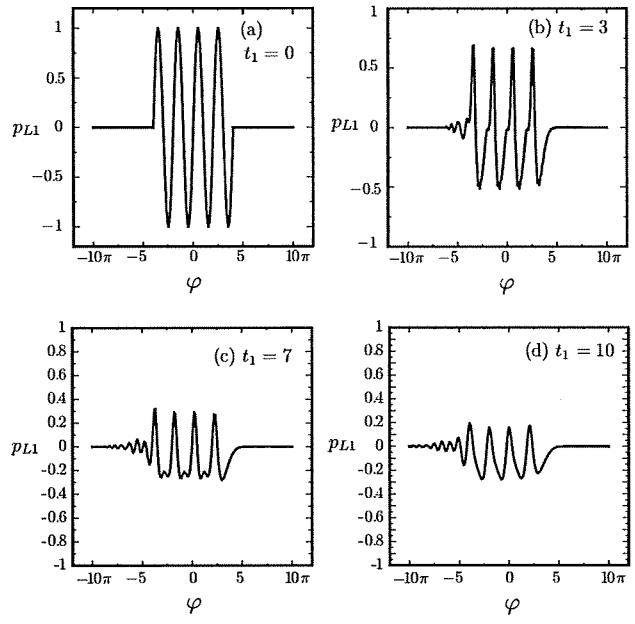

Figure 2. Wave profiles of the first-order liquid pressure p_{L1} in the case of $\alpha_0 = 0.02$, $\Delta = 0.1$, $\Omega = 0.4$, $V = 0.3$, $\beta_1 = \beta_2 = 0.5$, and $-10\pi \le \varphi \le 10\pi$: (a) $t_1 = 0$, (b) $t_1 = 3$, (c) $t_1 = 7$, (d) $t_1 = 10$.

we readily rewrite Eq. (49) into

$$\frac{\partial f}{\partial t_1} + C_1 f \frac{\partial f}{\partial \varphi} + C_2 \frac{\partial^2 f}{\partial \varphi^2} + C_3 \frac{\partial^3 f}{\partial \varphi^3} = 0. \tag{54}$$

Equation (54) is the so-called Korteweg–de Vries–Burgers equation (KdV–Burgers equation) [3]. The KdV–Burgers equation (54) describes the behavior of waves in the far field characterized by t_1 and φ, where the weak dissipation and weak dispersion effects appear and compete with the weak nonlinear effect.

In Fig. 2, we show some examples of time evolutions of wave profiles of the liquid pressure p_{L1}, evaluated by the numerical calculation of KdV–Burgers equation (54) with a finite difference method.

NONLINEAR WAVE OF STRONG DISPERSION

In this section, we focus on the moderately high frequency band, i.e., Band B in Fig. 1. Band B can be regarded as the strongly dispersive band. We shall study the nonlinear modulation of a quasi-monochromatic wave train in the long-range propagation of weakly nonlinear waves with a strong dispersion effect.

We shall define the scalings of parameters, as

$$\frac{U^*}{c_{L0}^*} \equiv O(\varepsilon^2) \equiv V\varepsilon^2, \tag{55}$$

$$\frac{R_0^*}{L^*} \equiv O(1) \equiv \Delta, \tag{56}$$

$$\frac{\omega^*}{\omega_B^*} \equiv T^*\omega^* \equiv O(1) \equiv \Omega, \tag{57}$$

where we determine $T^* \equiv 1/\omega_B^*$. The set of scalings (55)–(57) shows that the frequency is comparable with the eigenfrequency of bubble, the wavelength is also comparable with the initial bubble radius, and the propagation speed of waves is very small compared with the speed of sound in the liquid phase.

Although the method of averaged equation is usually prohibited to be applied to such short waves, the plane wave problem may be excluded from the restriction because the average volume can be sufficiently large along the plane parallel to the wave front [13]. Nevertheless, the assumption of spherical symmetry of bubble oscillations should be validated. We will address this problem in a future work.

Comparison of Eq. (24) with Eq. (55) yields $a = 5$, and therefore, in the present analysis, the liquid compressibility is assumed to be very small compared with the analysis in the previous section. Hence the expansions of the liquid density and pressure are, respectively, given as

$$\rho_L^*/\rho_{L0}^* = 1 + \varepsilon^5\rho_{L1} + \varepsilon^6\rho_{L2} + O(\varepsilon^7), \tag{58}$$

$$p_L = p_{L0} + \varepsilon p_{L1} + \varepsilon^2 p_{L2} + O(\varepsilon^3). \tag{59}$$

The expansion coefficients in Eq. (59) are defined by $p_{Lj} = \rho_{Lj}/V^2\,(j = 1, 2, 3, 4, 5)$. We therefore emphasis that the liquid compressibility cannot be neglected.

The analysis in this section requires t_1, t_2, x_1, and x_2 as the slow variables, and hence Eqs. (15) and (16), respectively, may be rewritten into

$$\frac{\partial}{\partial t} = \frac{\partial}{\partial t_0} + \varepsilon\frac{\partial}{\partial t_1} + \varepsilon^2\frac{\partial}{\partial t_2}, \tag{60}$$

$$\frac{\partial}{\partial x} = \frac{\partial}{\partial x_0} + \varepsilon\frac{\partial}{\partial x_1} + \varepsilon^2\frac{\partial}{\partial x_2}. \tag{61}$$

First-order equations

By using the same procedure as the derivation of Eq. (42) from Eqs. (37)–(41) in the previous section, we have the follow-

ing set of linear equations,

$$\frac{\partial \alpha_1}{\partial t_0} - 3\frac{\partial R_1}{\partial t_0} + \frac{\partial u_{G1}}{\partial x_0} = 0, \tag{62}$$

$$\alpha_0 \frac{\partial \alpha_1}{\partial t_0} - (1-\alpha_0)\frac{\partial u_{L1}}{\partial x_0} = 0, \tag{63}$$

$$\beta_1 \frac{\partial u_{G1}}{\partial t_0} - \beta_1 \frac{\partial u_{L1}}{\partial t_0} - 3\gamma p_{G0}\frac{\partial R_1}{\partial x_0} = 0, \tag{64}$$

$$(1-\alpha_0+\beta_1\alpha_0)\frac{\partial u_{L1}}{\partial t_0} - \beta_1\alpha_0\frac{\partial u_{G1}}{\partial t_0} + (1-\alpha_0)\frac{\partial p_{L1}}{\partial x_0} = 0, \tag{65}$$

$$\frac{\partial^2 R_1}{\partial t_0^2} + R_1 + \frac{p_{L1}}{\Delta^2} = 0, \tag{66}$$

and these can be reduced to the single equation

$$\mathcal{L}_1[R_1] = 0, \tag{67}$$

where the linear differential operator $\mathcal{L}_1$ is defined as

$$\mathcal{L}_1 \equiv \frac{\partial^2}{\partial t_0^2} - \left[\frac{\Delta^2}{3\alpha_0} + \frac{(1-\alpha_0+\beta_1)\gamma p_{G0}}{\beta_1(1-\alpha_0)}\right]\frac{\partial^2}{\partial x_0^2} - \frac{\Delta^2}{3\alpha_0}\frac{\partial^4}{\partial x_0^2 \partial t_0^2}. \tag{68}$$

Equation (67) corresponds to the linear wave equation with the dispersion term.

We take the solution of Eq. (67) as the form of a quasi-monochromatic wave train which evolves into a slowly modulated wave packet [18]:

$$R_1 = A(t_1, t_2, x_1, x_2)e^{i\theta} + \text{c.c.}, \tag{69}$$

with the phase function

$$\theta = k^* x_0^* - \omega^*(k^*)t_0^* = kx_0 - \Omega(k)t_0, \tag{70}$$

where A is the slowly varying complex amplitude which depends on t_1, t_2, x_1, and x_2, $k \equiv k^* L^*$ is the normalized wave number, i denotes the imaginary unit, and c.c. denotes the complex conjugate.

Note that the solution (69) describes a monochromatic wave train when A is independent of either t_1 and t_2 or x_1 and x_2.

The linear dispersion relation is obtained by substituting Eq. (69) into Eq. (67), as follows:

$$D(k,\Omega) = \frac{\Delta^2 k^2(1-\Omega^2)}{3\alpha_0} + \frac{(1-\alpha_0+\beta_1)\gamma p_{G0}}{\beta_1(1-\alpha_0)}k^2 - \Omega^2 = 0, \tag{71}$$

or

$$k = \pm\Omega\sqrt{\frac{3\alpha_0(1-\alpha_0)\beta_1}{3\alpha_0(1-\alpha_0+\beta_1)\gamma p_{G0} - \Delta^2\beta_1(1-\alpha_0)(\Omega^2-1)}}. \tag{72}$$

The cutoff frequency Ω_C is given as

$$\Omega_C = \sqrt{1 + \frac{3\alpha_0(1-\alpha_0+\beta_1)\gamma p_{G0}}{\beta_1(1-\alpha_0)\Delta^2}}. \tag{73}$$

The dispersion relations calculated from Eq. (71) are shown in Fig. 3.

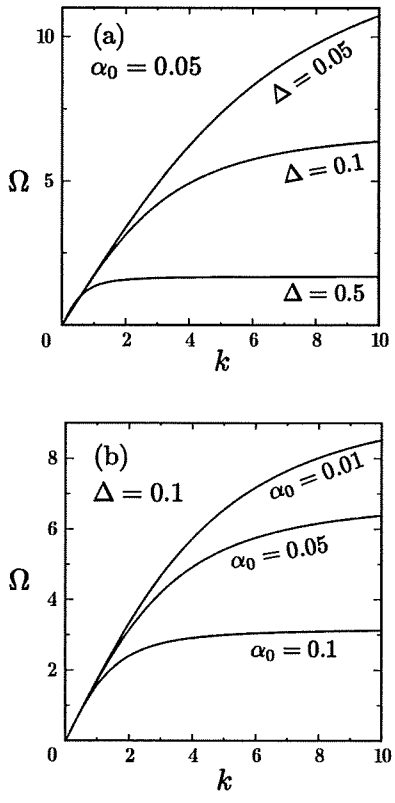

Figure 3. The dispersion relations in the bubbly liquid in the case of $\beta_1 = 0.5$, $\gamma = 1$, $p_{G0} = 1$, and typical values as follows: (a) $\alpha_0 = 0.05$: $\Delta = 0.05, 0.1, 0.5$; (b) $\Delta = 0.1$: $\alpha_0 = 0.01, 0.05, 0.1$.

Second-order equations

Substituting the solution (69) into the set of equations (62)–(66) and integrating them with respect to t_0 and x_0, we have α_1, u_{G1}, u_{L1}, and p_{L1} expressed by multiples of R_1. Then, the second-order equation is obtained as

$$\mathcal{L}_1[R_2] = H_2(x_0, x_1, t_0, t_1), \tag{74}$$

with the inhomogeneous term

$$H_2 = \Gamma A^2 e^{2i\theta} + i\left(-\frac{\partial D}{\partial \Omega}\right)\left(\frac{\partial A}{\partial t_1} + v_g \frac{\partial A}{\partial x_1}\right) e^{i\theta} + \text{c.c.}, \tag{75}$$

where Γ is a real constant.

From the non-secular condition of inhomogeneous equation (74), the second term in the right-hand side of Eq. (75) should vanish. We therefore obtain the following solvability condition

$$\frac{\partial A}{\partial t_1} + v_g \frac{\partial A}{\partial x_1} = 0. \tag{76}$$

Here, the normalized group velocity v_g is calculated by linear dispersion relation (71), as follows:

$$v_g = \frac{d\Omega}{dk} = \frac{3\alpha_0 \Omega(k)}{k(3\alpha_0 + \Delta^2 k^2)}. \tag{77}$$

The particular solution of Eq. (74) is given as

$$R_2 = \frac{\Gamma}{D(2k, 2\Omega)} A^2 e^{2i\theta} + \text{c.c.}. \tag{78}$$

As in the case of first-order equations, substituting the solution (78) into the set of equations of $O(\varepsilon^2)$ gives the explicit representations of α_2, u_{G2}, u_{L2}, and p_{L2}.

Third-order equations

Let us proceed to the next-order problem in order to determine the behavior of the slowly modulated wave packet as a result of long range propagation with weak nonlinear and strong dispersion effects.

The slightly lengthy calculations give the third-order equation

$$\mathcal{L}_1[R_3] = H_3(x_0, x_1, x_2, t_0, t_1, t_2), \tag{79}$$

with the inhomogeneous term

$$H_3 = \Gamma_1 e^{3i\theta} + \Gamma_2 e^{2i\theta} + \Gamma_3 e^{i\theta} + \Gamma_4 + \text{c.c.}, \tag{80}$$

where Γ_j $(j = 1, 2, 3, 4)$ are the complex variables including A and its derivatives. The explicit representation of Γ_3 is

$$\Gamma_3 = \left(-\frac{\partial D}{\partial \Omega}\right)\left[i\left(\frac{\partial A}{\partial t_2} + v_g \frac{\partial A}{\partial x_2}\right) + \frac{1}{2}\frac{dv_g}{dk}\frac{\partial^2 A}{\partial x_1^2} + \nu_1 |A|^2 A + i\nu_2 A\right]. \tag{81}$$

From the solvability condition of Eq. (79), we have

$$i\left(\frac{\partial A}{\partial t_2} + v_g \frac{\partial A}{\partial x_2}\right) + \frac{1}{2}\frac{dv_g}{dk}\frac{\partial^2 A}{\partial x_1^2} + \nu_1 |A|^2 A + i\nu_2 A = 0, \tag{82}$$

where the derivative dv_g/dk is calculated by the expression of group velocity (77), as

$$\frac{dv_g}{dk} = -\frac{9\alpha_0 \Delta^2 \Omega(k)}{(3\alpha_0 + \Delta^2 k^2)^2}, \tag{83}$$

and the real coefficient ν_2 is given as

$$\nu_2 = \frac{\Delta k^2}{2(3\alpha_0 + \Delta^2 k^2)}(4\mu + V\Delta^2), \tag{84}$$

and ν_2 has a positive value. The explicit representation of the real coefficient of the nonlinear term ν_1 is not shown here because of the complexity of expression.

By making use of the solvability conditions of the second-order (76) and the third-order (82), and the definitions of derivative expansions (60) and (61), we obtain

$$i\left(\frac{\partial A}{\partial t} + v_g \frac{\partial A}{\partial x}\right) + \frac{1}{2}\frac{dv_g}{dk}\frac{\partial^2 A}{\partial x^2} + \varepsilon^2(\nu_1 |A|^2 A + i\nu_2 A) = 0. \tag{85}$$

Furthermore, Eq. (85) can be rewritten into

$$i\frac{\partial A}{\partial \tau} + \frac{1}{2}\frac{dv_g}{dk}\frac{\partial^2 A}{\partial \xi^2} + \nu_1 |A|^2 A + i\nu_2 A = 0, \tag{86}$$

through the variable transformations

$$\tau \equiv \varepsilon^2 t = t_2, \quad \xi \equiv \varepsilon(x - v_g t) = x_1 - v_g t_1. \tag{87}$$

Equation (86) agrees with the well-known nonlinear Schrödinger equation [5, 8] if the coefficient ν_2 equals to zero. The fourth term in the left-hand side of Eq. (86) describes the attenuation effect of waves due to bubble oscillations. Therefore, Eq. (86) describes the behavior of the slowly modulated wave packet with the weak nonlinear, strong dispersion, and weak dissipation effects.

Let us put $A = ge^{ih}$, where g is the amplitude and h is the phase. Substituting it into Eq. (86) gives the following set of equations:

$$g\frac{\partial h}{\partial \tau} = \frac{1}{2}\frac{dv_g}{dk}\left[\frac{\partial^2 g}{\partial \xi^2} - g\left(\frac{\partial h}{\partial \xi}\right)^2\right] + \nu_1 g^3, \tag{88}$$

$$\frac{\partial g}{\partial \tau} = -\frac{1}{2}\frac{dv_g}{dk}\left[g\frac{\partial^2 h}{\partial \xi^2} + 2\left(\frac{\partial g}{\partial \xi}\right)\left(\frac{\partial h}{\partial \xi}\right)\right] - \nu_2 g. \tag{89}$$

We shall solve the set of equations (88) and (89) with a finite difference method. Figures 4 and 5 show some examples of the time evolutions of the amplitude g and phase h, where the coefficients ν_1 and ν_2 are selected as specific values.

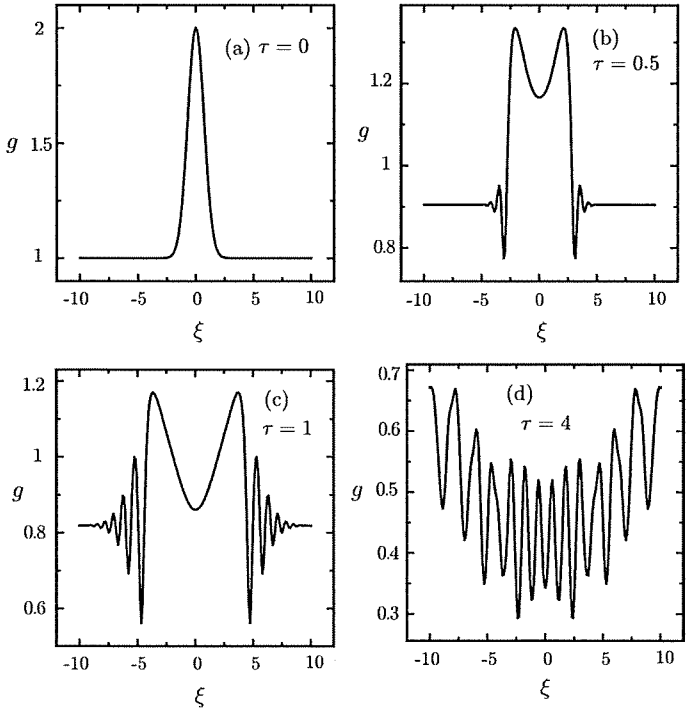

Figure 4. The profiles of the amplitude g in the case of $\nu_1 = 4$, $\nu_2 = 0.2$, $dv_g/dk = -1$, and $-10 \le \xi \le 10$: (a) $\tau = 0$, (b) $\tau = 0.5$, (c) $\tau = 1$, (d) $\tau = 4$.

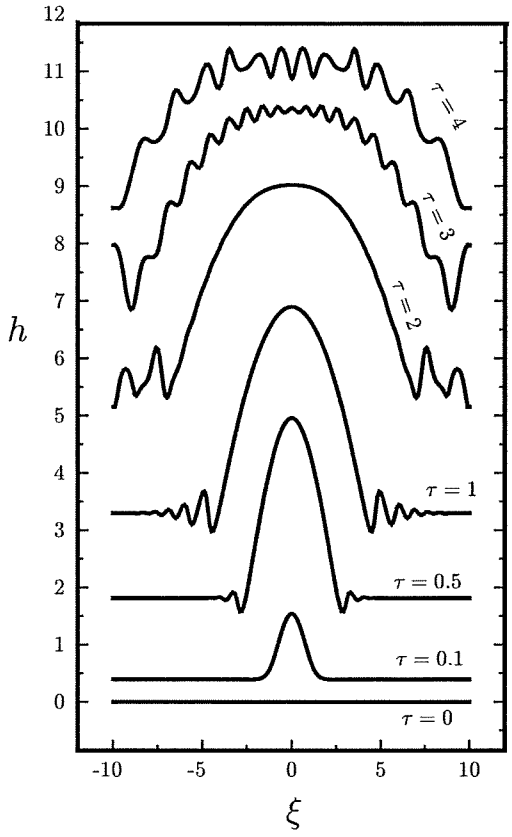

Figure 5. The profiles of the phase h in the case of $\nu_1 = 4$, $\nu_2 = 0.2$, $dv_g/dk = -1$, and $-10 \le \xi \le 10$: $\tau = 0, 0.1, 0.5, 1, 2, 3, 4$.

CONCLUSION

The weakly nonlinear analyses of pressure waves in bubbly liquids have been carried out based on the two-fluid averaged equations. We have derived the equations describing wave motions in far fields by the use of the method of multiple scales and the appropriate scaling of parameters.

In the moderately low frequency band, the KdV–Burgers equation describes the behavior of waves in the far field, where the weak dissipation and weak dispersion effects appear and compete with the weak nonlinear effect.

In the moderately high frequency band, the nonlinear Schrödinger equation with the attenuation term can be derived as the far field equation of the quasi-monochromatic wave train. It describes the weakly nonlinear modulation with the weak dissipation effect, caused by the strong dispersion effect.

ACKNOWLEDGEMENTS

This work was carried out by the aid of Research on Advanced Medical Technology, Ministry of Health, Labor and Welfare (H19-nano-010). The authors would like to express their deepest gratitude towards this grant.

REFERENCES

[1] Tangren, R. F., Dodge, C. H. and Seifert, H., *J. Appl. Phys.*, **20**, 637 (1949).
[2] van Wijingaarden, L., *J. Fluid Mech.*, **33**, 465 (1968).
[3] van Wijingaarden, L., *Ann. Rev. Fluid Mech.*, **4**, 369 (1972).
[4] Caflisch, R. E., Miksis, M. J., Papanicolaou, G. C. and Ting, L., *J. Fluid Mech.*, **153**, 259 (1985).
[5] Gumerov, N. A., *J. Appl. Math. Mech.*, **56**, 50 (1992).
[6] Watanabe, M. and Prosperetti, A., *J. Fluid Mech.*, **274**, 349 (1994).
[7] Kameda, M. and Matsumoto, Y., *Phys. Fluids*, **8**, 322 (1996).
[8] Khismatullin, D. B. and Akhatov, I. Sh., *Phys. Fluids*, **13**, 3582 (2001).
[9] Preston, A. T., Colonius, T. and Brennen, C. E., *Phys. Fluids*, **14**, 300 (2002).
[10] Matsumoto, Y. and Yoshizawa, S., *Int. J. Numer. Meth. Fluids*, **47**, 591 (2005).
[11] Egashira, R., Yano, T. and Fujikawa, S., *Fluid Dyn. Res.*, **34**, 317 (2004).
[12] Yano, T., Egashira, R. and Fujikawa, S., *J. Phys. Soc. Jpn.*, **75**, 104401 (2006).
[13] Haga, T., Yano, T. and Fujikawa, S., *Proceedings of the 7th JSME-KSME Thermal and Fluids Engineering Conference*, Japan (2008).
[14] Jeffrey, A. and Kawahara, T., *Asymptotic Methods in Nonlinear Wave Theory*, (Pitman Advanced Pub. Program, Boston, 1982).
[15] Zhang, D. Z. and Prosperetti, A., *J. Fluid Mech.*, **267**, 185 (1994).
[16] Eames, I. and Hunt, J. C. R., *J. Fluid Mech.*, **505**, 349 (2004).
[17] Keller, J. B. and Kolodner, I. I., *J. Appl. Phys.*, **27**, 1152 (1956).
[18] Nayfeh, A. H., *J. Acoust. Soc. Am.*, **57**, 803 (1975).

Tohoku J. Exp. Med., 2009, 217, 185-191

Cysteinyl Leukotrienes Enhance the Degranulation of Bone Marrow-Derived Mast Cells through the Autocrine Mechanism

Izumi Kaneko,[1] Kaori Suzuki,[2] Kaori Matsuo,[3] Hiroyuki Kumagai,[1] Yuji Owada,[4] Naoya Noguchi,[5] Takanori Hishinuma[6,*] and Masao Ono[1]

[1]Department of Pathology, Tohoku University Graduate School of Medicine, Sendai, Japan
[2]Division of Clinical Pharmacy, Tohoku University Graduate School of Pharmaceutical Sciences, Sendai, Japan
[3]Division of Biomedical Engineering for Health and Welfare, Tohoku University Graduate school of Biomedical Engineering, Sendai, Japan
[4]Department of Organ Anatomy, Yamaguchi University Graduate School of Medicine, Ube, Japan
[5]Department of Biochemistry, Tohoku University Graduate School of Medicine, Sendai, Japan
[6]Division of Pharmacotherapy, Tohoku University Graduate School of Pharmaceutical Sciences, Sendai, Japan

The cysteinyl leukotrienes (LTs), LTC_4, LTD_4, and LTE_4, are potent inflammatory mediators and are involved in allergic reactions, such as bronchoconstriction, eosinophilic inflammation, and allergic cell proliferation. The present study aimed to elucidate the role of constitutively produced cysteinyl LTs in mast cell activation. We used a newly developed quantification method based on mass spectrometry to detect cysteinyl LTs in the cultured medium of mouse bone marrow-derived mast cells (BMMCs), which were obtained by interleukin (IL)-3-conditioned culture of mouse bone marrow. BMMCs were stimulated with immunoglobulin (Ig) E and antigen (IgE/Ag) or lipopolysaccharide for 1 or 24 h. This new quantification method revealed that unstimulated BMMCs produced and secreted LTB4 and LTE4 after 24 h of incubation. The treatment of unstimulated BMMCs for 2 h with montelukast, an antagonist of a cysteinyl LT receptor, CysLT1, resulted in the suppression of a downstream signaling event of this receptor, i.e., the decrease in phosphorylation of extracellular responsive kinases. Thus, cysteinyl LTs constitutively simulate BMMCs through the CysLT1 receptor in an autocrine manner. Treatment of BMMCs for 3 weeks with montelukast, which caused long-term inhibition of the autocrine cyteinyl LT-derived signal, significantly attenuated the IgE/Ag-dependent degranulation, as judged by the decrease in the release of β-hexosaminidase, an enzyme contained in the granules, whereas the production of cytokines, such as IL-6 and tumor necrosis factor-α, were largely unaffected. In conclusion, an autocrine signal derived from constitutively produced cysteinyl LTs predisposes mast cells to the degranulation upon allergic stimulation. ——— autocrine; CysLT1; cysteinyl leukotriene; mast cell; montelukast.
Tohoku J. Exp. Med., 2009, 217 (3), 185-191.

The cysteinyl leukotrienes (LTs), LTC_4, LTD_4, and LTE_4 are potent inflammatory mediators that are synthesized from the membrane lipid component arachidonic acid and are involved in several types of pathophysiological inflammations. Cysteinyl LTs are released from leukocytes in the early phase of the inflammatory response and serve as contractile agonists for tissues that contain smooth muscles, such as blood vessels and bronchi. Besides their role as contractile agonists, cysteinyl LTs stimulate various cells and exert pleiotropic effects such as hematopoiesis, cellular migration (Bautz et al. 2001), leukocyte adhesion to endothelial cells (Kanwar et al. 1995; Pedersen et al 1997; Nagata et al. 2002; Di Gennaro et al. 2004), chemoattraction (Laitinen et al. 1993; Spada et al. 1994), cell proliferation, and cell survival (Jiang et al. 2006; Vannella et al. 2007; Bosse et al. 2008). In the pathological context, cysteinyl LTs play important roles in the manifestation of allergic symptoms; therefore, receptor antagonists against cysteinyl LTs are widely used for anti-allergic therapy.

The G-protein-coupled receptors CysLT1 and CysLT2 have been characterized as selective receptors for cysteinyl LTs (Lynch et al. 1999; Heise et al. 2000). It has been shown that CysLT1 mediates activation signals, whereas CysLT2 down-modulates the CysLT1-mediated signals (Jiang et al. 2007). Furthermore, the cellular and tissue distribution patterns of these receptors are different. It was found that the brain and heart express CysLT2, whereas blood leukocytes and mast cells express both CysLT1 and

Received November 20, 2008; revision accepted for publication January 31, 2009.
*This work is dedicated to the memory of Takanori Hishinuma who initiated this project.
Correspondence: Masao Ono, M.D., Department of Pathology, Tohoku University Graduate School of Medicine, 2-1 Seiryo, Aoba-ku, Sendai, Miyagi 980-8575, Japan.
e-mail: onomasao@mail.tains.tohoku.ac.jp

CysLT2 (Mellor et al. 2001; Bautz et al. 2001; Figueroa et al. 2003; Mellor et al. 2003). Mice lacking the LTC_4 synthetase, an enzyme that is required for the synthesis of all cysteinyl LTs, show markedly attenuated mast cell hyperplasia in response to an allergenic challenge (Kim et al. 2006); this suggests that CysLT1 and/or CysLT2 play a critical role in the development or migration of mast cells in vivo.

Mast cells are critical for the initiation of allergic diseases: they detect allergens, release early inflammatory mediators such as histamine, and mediate the type 2 helper T cell (T_h2) response by releasing cytokines. In light of the importance of lipid mediators in the onset of allergic reactions, we have investigated their roles in mast cell activation by using bone marrow-derived, Interleukin (IL)-3-dependent mast cells (BMMCs) (Kaneko et al. 2008). In the initial phase of the present study, we detected cysteinyl LTs in the cultured medium of unstimulated BMMCs by using a new method based on mass spectrometry. This finding, in turn, raised a new question about the biological significance of the constitutive production of cysteinyl LTs in the function of BMMCs. The present findings provide a new insight into the important role of CysLT1-mediated signals in mast cell exocytosis.

Materials and Methods

Mast cell culture and activation

Bone marrow cells were prepared from 2 to 3 month-old C57BL/6J and MRL/Mp mice (Charles River Breeding Laboratories, Yokohama, Japan). BMMCs were obtained by a long-term culture (>3 weeks) of mouse bone marrow cells in the RPMI 1640 medium supplemented with 10% fetal calf serum (FCS), 1 mM sodium pyruvate, non-essential amino acids, 50 μM 2-mercaptoethanol (SIGMA, St. Louis, MO), and 5 ng/ml murine IL-3 (R&D Systems, Minneapolis, MN). BMMCs (10^5 cells/200 μl) were activated with 1 μg/ml trinitrophenyl (TNP)-specific immunoglobulin (Ig) E (TNP-IgE) and 0.1-30 ng/ml of TNP-conjugated ovalbumin (TNP-OVA) (fraction VII, SIGMA). Lipopolysaccharide (LPS; *Escherichia coli* 055:B5; SIGMA) was used for stimulation at a concentration of 0.1 or 1 μg/ml. An antagonist of CysLT1, montelukast, which was kindly donated by Merck Co. Ltd., was supplemented into the culture at 1 or 10 μM for 2 h or 3 weeks before activation. During the long-term culture of BMMCs with montelukast, the medium was replaced twice a week with fresh medium supplemented with montelukast.

Liquid chromatography/tandem mass spectrometry (LC/MS-MS) analysis

The simultaneous quantification of LTs was performed using the cultured medium collected at 1 h or 24 h after the stimulation. LTB_4-d_4 (Cayman chemical, Ann Arbor, MI), LTC_4-d_3, LTD_4-d_3, and LTE_4-d_3 (BIOMOL, Plymouth Meeting, PA) (each 2 ng) were added into the cultured medium (0.1 ml) as internal standards. The sample was acidified and passed through an Empore C18 HD disk cartridge (3 M Industry, St. Paul, MN). The bound fraction was collected in acetonitrile-water (3:7, v/v; 1 ml) as the LT-enriched fraction. After evaporating the solvent, the residue was reconstituted in the mobile phase (40 μl), sonicated for 30 s, and filtered. The reconstituted sample was transferred to an autosampler vial; 10 μl of the sample was subjected to the LC/MS-MS analysis. The high-performance liquid chromatography (HPLC) was performed in a Capcell Pak C18 MGII column (1.5 × 150 mm; 5 μm) (Shiseido, Tokyo, Japan) using gradient elution with acetonitrile (solvent A) and 5 mM ammonium acetate (solvent B) at a flow rate of 200 μl/min at 40°C. The gradient was set up as follows: the fraction of solvent A was increased from 23% to 53% in 3 min and then maintained at 53% for 6 min. The LC/MS/MS analysis was performed using a TSQ Quantum Ultra triple quadrupole mass spectrometer (Thermo Fisher, Waltham, MA) equipped with an electrospray ion source and operated in the negative-ion mode. Using selected reaction monitoring (SRM), transitions of *m/z* 335 to 195, *m/z* 624 to 272, *m/z* 495 to 177, and *m/z* 438 to 333 were used for the measurement of LTB_4-d_4, LTC_4-d_3, LTD_4-d_3, and LTE_4-d_3, respectively.

Activation of extracellular signal-regulated kinases (ERKs)

The activities of ERKs 1/2, which are known to be phosphorylated on receiving signals via CysLT1, were monitored by the detection of their phosphorylated form with western blot analysis and flow cytometry. For the western blot analysis, BMMCs (5×10^6) were suspended on ice in 100 μl radioimmunoprecipitation assay (RIPA) buffer containing 20 mM Tris-Cl (pH 7.4), 150 mM NaCl, 1 mM EDTA, 1% (v/v) Triton X-100, 0.5% (w/v) sodium deoxycholate, 1 mM phenylmethylsulphonyl fluoride (PMSF), and 1× phosphatase inhibitor cocktail (Sigma). The postnuclear fraction was mixed with sodium dodecyl sulphate (SDS) sample buffer and denatured in boiled water for 5 min. A sample volume containing 5×10^5 cells was fractionated on a polyacrylamide gel (12.5%) containing SDS and transferred to a polyvinylidene difluoride membrane (Millipore, Bedford, MA). An affinity-purified antibody to ERK1/2 (Santa Cruz, Santa Cruz, CA) and a rabbit monoclonal antibody to phospho-ERK1/2 (pERK1/2) (T202/Y204) (Cell Signaling, Danvers, MA) were used as the primary antibodies. In the flow cytometry, BMMCs (10^6) were treated with montelukast or the mitogen-activated protein kinase kinase-1 inhibitor PD98059 for 2 h and fixed in phosphate-buffered 2% paraformaldehyde for 30 min at room temperature; this was followed by further incubation in 90% ice-cold ethanol for 15 min to allow the antibodies to permeate the cells. The primary antibody anti-pERK1/2 antibody (T202/Y204) (Cell Signaling Tech, Danvers, MA) and the secondary antibody Alexa 594-conjugated anti-rabbit antibody were serially used for immunostaining.

Cytokine release and degranulation of BMMCs

The concentrations of IL-6 and tumor necrosis factor (TNF)-α in the cultured medium collected at 6 h after the stimulation were determined by enzyme-linked immunosorbent assay (ELISA) kits (BD PharMingen, San Diego, CA). The degranulation response of BMMCs was quantified by determining the fraction of released β-hexosaminidase or histamine in the cultured medium as previously described (Ono et al. 1999). Histamine concentration was measured using the histamine ELISA kit (Neogen, Lexington, KY). The percent degranulation of BMMC was estimated by the following formula: 100 × (β-hexosaminidase activity or histamine in the supernatant fraction)/(total β-hexosaminidase activity or histamine in the cellular and supernatant fractions).

Statistical analysis

The difference between 2 mean values was evaluated by the

TABLE 1. Cumulative amount of leukotrienes in BMMC cultured medium[a].

Treatment	LTB4	LTC4	LTD4	LTE4
For 1 h		(ng/10^5 cells)		
untreated	n.d.	n.d.	n.d.	n.d.
LPS	n.d.	n.d.	n.d.	n.d.
IgE/Ag	8.15 (7.67)	6.03 (8.56)	2.94 (2.08)	33.1 (28.2)
For 24 h				
untreated	2.21 (1.90)	n.d.	n.d.	14.7 (6.85)
LPS	n.d.	n.d.	n.d.	n.d.
IgE/Ag	5.09 (2.87)	n.d.	n.d.	34.2 (27.4)

[a]Each value denotes a mean (standard deviation: S.D.) of the concentration of three samples in a single experiment, each of which was independently treated. BMMCs were stimulated without (untreated) or with 0.1 μg/ml LPS (LPS), or 1 ng/ml TNP-OVA following IgE sensitization (IgE/Ag). Culture supernatants were collected at 1 h (For 1 h) or 24 h (For 24 h) after stimulation.

LT, leukotriene; n.d., not detected.

two-tailed *t* test. *P* value less than 0.05 was regarded as significant.

RESULTS AND DISCUSSION

Constitutive production of cysteinyl LTs and LTB$_4$ in the BMMCs

We have previously shown that the autocrine release of constitutively produced prostanoid species significantly contributes to mast cell activation (Kaneko et al. 2008). In this previous study, we also demonstrated the suppressive effect of a 5-lipoxygenase (5-LO) inhibitor, nordihydroguaiaretic acid, on the cytokine responses mediated by BMMCs. These findings have provided a better understanding of the role of 5-LO metabolites and prostanoids in BMMC activation. To identify the individual LTs liberated from the BMMCs and to quantify each LT, we developed a new highly sensitive and specific method for the simultaneous determination of the amounts of LTB_4, LTC_4, LTD_4, and LTE_4 in the cultured medium. We used 3 culture conditions: no treatment, treatment with LPS (100 ng/ml), and treatment with IgE plus antigen (IgE/Ag) (1 ng/ml TNP-OVA). All the LTs were detected in the culture medium 1 h after the treatment with IgE/Ag, but LTs were not detected after the treatment with LPS (Table 1), despite that LPS increased cytokine production in BMMCs under certain conditions (Kaneko et al. 2008). Notably, 24 h after the treatment, LTB_4 and LTE_4 were detected in the culture media of untreated BMMCs and IgE/Ag-stimulated BMMCs. LTC_4 and LTD_4 were not detected in the cultured medium at 24 h probably because they were metabolically converted to LTE_4. These findings indicate that BMMCs synthesize LTB4 and other cysteinyl LTs independent of stimulation.

At a concentration of 10 nM, cysteinyl LTs are known to influence the signaling events in mast cells: calcium influx, the activation of the mitogen-activated protein kinase pathway, production of cytokines and chemokines, and internalization of the c-KIT receptor (Jiang et al. 2007). In the present study, the LTE_4 concentration in the cultured media after 24 h was as high as 170 nM, which is comparable to the LTE_4 concentrations that generally initiate signaling events. These findings suggest an interesting possibility that the autocrine secretion of constitutively expressed cysteinyl LTs influences BMMC functions.

Constitutive cysteinyl LTs in BMMC culture activate ERKs via CysLT1

We examined whether cysteinyl LTs affected the signal transduction in BMMCs under the untreated condition. CysLT1-mediated signals were assessed by comparing the active state of ERK1/2, which is reflected by pERK1/2, in the presence or absence of the CysLT1 antagonist montelukast, which affects the signaling events downstream of CysLT1. pERK1/2 was detected using western blot analysis with an anti-ERK1/2 antibody (Fig. 1A) and flow cytometric analysis (Fig. 1B). We found that the amount of pERK1/2 after treatments with 1 or 10 μM montelukast was lower than the amount in untreated cells. BMMC proliferation was not affected by treatment with 1 μM montelukast, but it was marginally suppressed by treatment with 10 μM montelukast (data not shown). These findings suggest that the constitutively produced cysteinyl LTs present in the untreated condition participated in CysLT1-mediated signal transduction in BMMCs.

Constitutive CysLT1-mediated signals affect the degranulation of BMMCs

In order to test the hypothesis that the CysLT1-mediated signals influence BMMC functions in an autocrine manner, we quantified the degranulation (Fig. 2A-E) and cytokine production (Fig. 2F and G) under 3 conditions: no treatment, treatment with montelukast (1 or 10 μM) for 2 h, and treatment with montelukast for 3 weeks. To distinguish

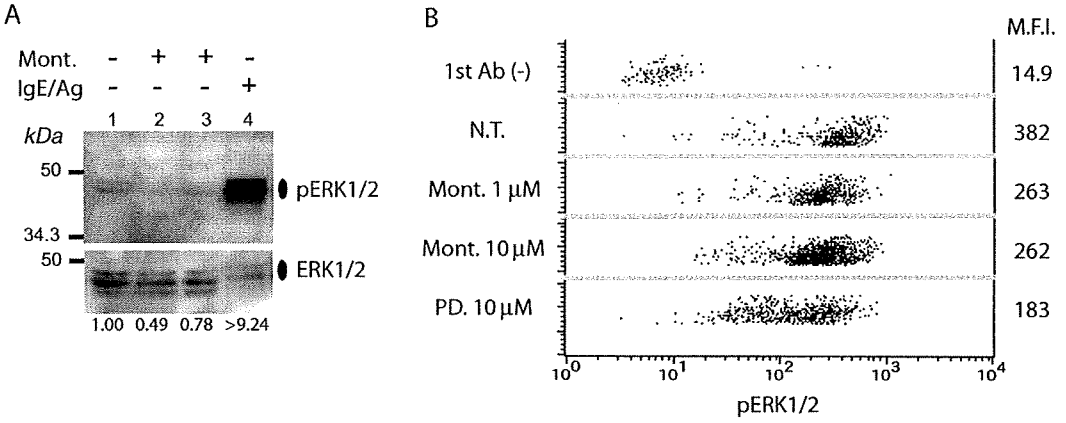

Fig. 1. Effect of CysLT1 inhibition by montelukast on ERK1/2 phosphorylation in BMMCs. (A) pERK1/2 detected by western blot analysis with anti-pERK1/2 antibody. The level of pERK1/2 decreased after the incubation of BMMCs with 1 μM (lane *2*) or 10 μM (lane *3*) montelukast for 2 h as compared to the levels in untreated BMMCs (lane *1*). The level of pERK1/2 induced by IgE/Ag stimulation is also shown (lane *4*). Values at the bottom of the figure represent the fraction of the signal intensity of the treated samples compared to that of the untreated sample. (B) Flow cytometric detection of pERK1/2. Treatment with montelukast (*Mont. 1 or 10 μM*) or PD98059 (*PD. 10 μM*) reduced the level of pERK1/2. *1st Ab (–)*, omission of incubation with primary antibody; *N.T.*, not treated. We confirmed these changes in the level of pERK1/2 by performing another experiment involving western blot and flow cytometric analysis.

the effects of the treatment on the early and late stages of BMMC development, the treatments were administered on a preparation of immature BMMCs (at the third week of culture) and a preparation of mature BMMCs (at the sixth week of culture). The degranulation induced on IgE/Ag stimulation was assessed by determining the fraction of released β-hexosaminidase, an enzyme present in granules (Fig. 2A and B), or histamine (Fig. 2C–E). The β-hexosaminidase assays revealed that the long-term treatment significantly suppressed the degranulation, whereas the short-term treatment did not suppress it. The histamine assays revealed the same tendency as observed in the β-hexosaminidase assays, although statistical significance was not evident probably owing to the small number of samples examined. Further, the results were similar for both mature and immature BMMCs. The total amounts of β-hexosaminidase (data not shown) and histamine (Fig. 2C) were not altered in either condition. These results indicate that the efficacy of CysLT1 receptor antagonism critically differs according to the period of the treatment. In contrast, the production of IL-6 (Fig. 2F) and TNF-α (Fig. 2G) after IgE/Ag stimulation was not influenced by CysLT1 antagonism. The expression of the c-KIT and Fc receptors for IgE (Fcε RI) remained unaltered after the long-term treatment (data not shown). Collectively, these findings show that in BMMCs, constitutively produced cysteinyl LTs play a substantial role in the development of exocytosis, which is a fundamental function of mast cells.

Mast cells are known to robustly produce cysteinyl LTs upon inflammatory stimulation and bear the cysteinyl LT receptors CysLT1 and CysLT2. The role of autocrine secretion of constitutively produced cysteinyl LTs in mast cell functions has been shown by using BMMCs grown in the presence of stem cell factor (SCF) and IL-4 (Jiang et al. 2006). This previous study has shown that the genetic depletion of CysLT1 in BMMCs or treatment of BMMCs with MK571, a CysLT1 antagonist, markedly attenuates their proliferation with reduced phosphorylation of ERK1/2. The present study revealed that CysLT1 antagonism has little effect on the proliferation of BMMCs. The difference between the present and previous results with respect to the effect of CysLT1-mediated signals on cell proliferation is probably attributable to the difference in the growth conditions. SCF and IL-4 were used in the previous study, while IL-3 was used in the present study. Nevertheless, cysteinyl LTs can be considered to be occasionally or constitutively present in the mast cell microenvironment independent of the growth condition.

It has been shown that transient signals via CysLT1 and CysLT2 lead to activation of mast cell that revealed by calcium influx, activation of the mitogen-activated protein kinase pathway, and production of cytokines and chemokines (Mellor et al. 2001; Lin and Boyce, 2005; Paruchuri et al. 2008). A previous report has revealed an effect of montelukast on mast cell function other than its primary effect, i.e., CysLT1 antagonism (Ramires et al. 2004). In this previous study, montelukast was shown to serve as an inhibitor of 5-LO, which is an enzyme essential for the in vivo synthesis of leukotriene species. In contrast to an increasing amount of information regarding the effects of the temporal activation of CysLT1 and/or CysLT2, little information is available regarding the chronic effects of CysLT1- and/or CysLT2-mediated signals. We showed for the first time the remarkable chronic effects of these signals on mast cell activation. These constitutive signals seem to be involved in the initiation of degranulation but not cytokine production in mast cells. This fact clearly depicts a distinct difference between the effects of temporal and chronic CysLT1-

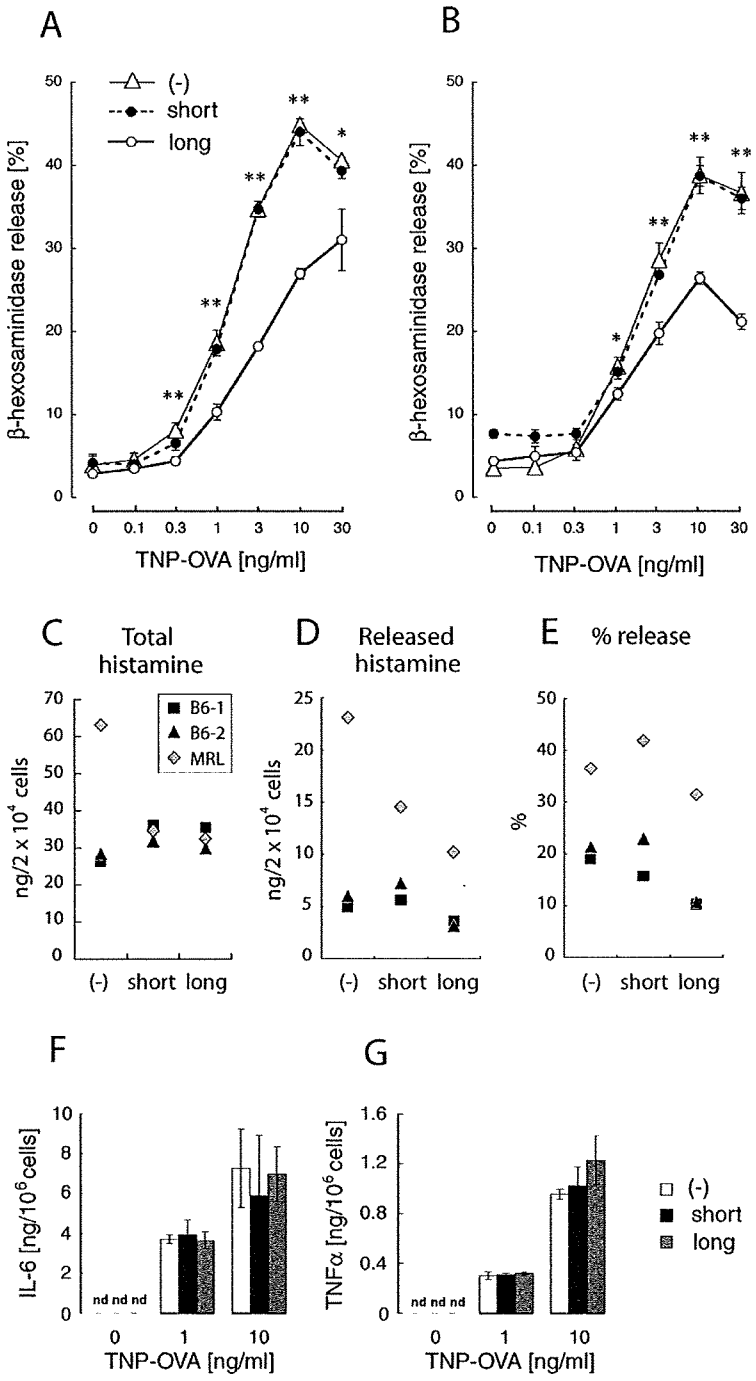

Fig. 2. Blocking of the exocytotic response of BMMCs to crosslinking of FcεRI via CysLT1 inhibition. (A, B) Effect of treatment with 10 μM montelukast on β-hexosaminidase release from immature BMMCs (A) or mature BMMCs (B), which were stimulated at the end of the third or sixth week, respectively, of bone marrow culture. The average percent release of triplicate samples is shown. *(–)*, no treatment (triangle); *short*, short-term (2 h) treatment (filled circle); *long*, long-term treatment (open circle). These results were reproduced in a second experiment performed using independently prepared samples. (C–E) Effect of treatment with 1 μM montelukast on total (cellular and released) histamine (C), released histamine (D), and percent fraction of the released histamine (E). The results obtained from 3 independent BMMC preparations are shown. *B6-1*, a B6 mouse (filled square); *B6-2*, another B6 mouse (filled triangle); *MRL*, an MRL mouse (open diamond). (F, G) Effects on the production of IL-6 (F) and TNF-α (G) in BMMCs. The same samples as in B were used for these measurements. Bars represent the standard deviation (S.D.) of triplicate samples. Asterisk(s) at each dose of antigen indicates (indicate) significant difference between *(–)* and *long*. $*p < 0.05$; $**p < 0.01$.

and/or CysLT2-mediated signals. It is important to understand how the chronic signal participates in a distinct molecular mechanism for mast cell degranulation.

Concluding Remarks

Cysteinyl LTs are known to be critical mediators of inflammation, and their roles in pathological inflammatory conditions such as asthma have been elucidated. The present study revealed a novel mode—an autocrine, constitutive mode—of cysteinyl LT production in mast cells. Furthermore, the present experiments conducted using BMMCs showed that the autocrine secretion of constitutively produced cysteinyl LTs leads to chronic effects on mast cell degranulation, which is related to pro-allergic conditions. Targeted inhibition of CysLT1 has been established as an efficacious therapy for the treatment of these conditions. Since CysLT1 is expressed in a broad range of cell types, including epithelial cells, endothelial cells, smooth muscle cells, and most leukocytes, the net outcome of CysLT1 inhibition, i.e., the suppression of the functions of these cell types, is considered to be beneficial. Mast cells have been shown to potentially undergo a self-conditioning toward the onset of allergic symptoms. Hence, mast cells in the subclinical condition of allergic diseases are also important targets for CysLT1 inhibition during allergic therapy.

Acknowledgments

The authors thank Profs. N. Mano and S. Takasawa for providing us with valuable suggestions, Mrs. F. Date for technical assistance, and Mrs. E. Yura for secretarial assistance. This study was supported by a research grant from Merck and Grants-in-Aid for Scientific Research from the Ministry of Education, Science, Sports, and Culture of Japan to M.O.

References

Bautz, F., Denzlinger, C., Kanz, L. & Mohle, R. (2001) Chemotaxis and transendothelial migration of CD34(+) hematopoietic progenitor cells induced by the inflammatory mediator leukotriene D4 are mediated by the 7-transmembrane receptor CysLT1. *Blood*, **97**, 3433-3440.

Bosse, Y., Thompson, C., McMahon, S., Dubois, C.M., Stankova, J. & Rola-Pleszczynski, M. (2008) Leukotriene D4-induced, epithelial cell-derived transforming growth factor beta1 in human bronchial smooth muscle cell proliferation. *Clin. Exp. Allergy*, **38**, 113-121.

Di Gennaro, A., Carnini, C., Buccellati, C., Ballerio, R., Zarini, S., Fumagalli, F., Viappiani, S., Librizzi, L., Hernandez, A., Murphy, R.C., Constantin, G., De Curtis, M., Folco, G. & Sala, A. (2004) Cysteinyl-leukotrienes receptor activation in brain inflammatory reactions and cerebral edema formation: a role for transcellular biosynthesis of cysteinyl-leukotrienes. *FASEB J.*, **18**, 842-844.

Figueroa, D.J., Borish, L., Baramki, D., Philip, G., Austin, C.P. & Evans, J.F. (2003) Expression of cysteinyl leukotriene synthetic and signalling proteins in inflammatory cells in active seasonal allergic rhinitis. *Clin. Exp. Allergy*, **33**, 1380-1388.

Heise, C.E., O'Dowd, B.F., Figueroa, D.J., Sawyer, N., Nguyen, T., Im, D.S., Stocco, R., Bellefeuille, J.N., Abramovitz, M., Cheng, R., Williams, D.L. Jr., Zeng, Z., Liu, Q., Ma, L., Clements, M.K., Coulombe, N., Liu, Y., Austin, C.P., George, S.R., O'Neill, G.P., Metters, K.M., Lynch, K.R. & Evans, J.F. (2000) Characterization of the human cysteinyl leukotriene 2 receptor. *J. Biol. Chem.*, **275**, 30531-30536.

Jiang, Y., Borrelli, L.A., Kanaoka, Y., Bacskai, B.J. & Boyce, J.A. (2007) CysLT2 receptors interact with CysLT1 receptors and down-modulate cysteinyl leukotriene dependent mitogenic responses of mast cells. *Blood*, **110**, 3263-3270.

Jiang, Y., Kanaoka, Y., Feng, C., Nocka, K., Rao, S. & Boyce, J.A. (2006) Cutting edge: Interleukin 4-dependent mast cell proliferation requires autocrine/intracrine cysteinyl leukotriene-induced signaling. *J. Immunol.*, **177**, 2755-2759.

Kaneko, I., Hishinuma, T., Suzuki, K., Owada, Y., Kitanaka, N., Kondo, H., Goto, J., Furukawa, H. & Ono, M. (2008) Prostaglandin F2α regulates cytokine responses of mast cells through the receptors for prostaglandin E. *Biochem. Biophys. Res. Commun.*, **367**, 590-596.

Kanwar, S., Johnston, B. & Kubes, P. (1995) Leukotriene C4/D4 induces P-selectin and sialyl Lewis(x)-dependent alterations in leukocyte kinetics in vivo. *Circ. Res.*, **77**, 879-887.

Kim, D.C., Hsu, F.I., Barrett, N.A., Friend, D.S., Grenningloh, R., Ho, I.C., Al-Garawi, A., Lora, J.M., Lam, B.K., Austen, K.F. & Kanaoka, Y. (2006) Cysteinyl leukotrienes regulate Th2 cell-dependent pulmonary inflammation. *J. Immunol.*, **176**, 4440-4448.

Laitinen, L.A., Laitinen, A., Haahtela, T., Vilkka, V., Spur, B.W. & Lee, T.H. (1993) Leukotriene E4 and granulocytic infiltration into asthmatic airways. *Lancet*, **341**, 989-990.

Lin, D.A. & Boyce, J.A. (2005) IL-4 regulates MEK expression required for lysophosphatidic acid-mediated chemokine generation by human mast cells. *J. Immunol.*, **175**, 5430-5438.

Lynch, K.R., O'Neill, G.P., Liu, Q., Im, D.S., Sawyer, N., Metters, K.M., Coulombe, N., Abramovitz, M., Figueroa, D.J., Zeng, Z., Connolly, B.M., Bai, C., Austin, C.P., Chateauneuf, A., Stocco, R., Greig, G.M., Kargman, S., Hooks, S.B., Hosfield, E., Williams, D.L. Jr., Ford-Hutchinson, A.W., Caskey, C.T. & Evans, J.F. (1999) Characterization of the human cysteinyl leukotriene CysLT1 receptor. *Nature*, **399**, 789-793.

Mellor, E.A., Frank, N., Soler, D., Hodge, M.R., Lora, J.M., Austen, K.F. & Boyce, J.A. (2003) Expression of the type 2 receptor for cysteinyl leukotrienes (CysLT2R) by human mast cells: Functional distinction from CysLT1R. *Proc. Natl. Acad. Sci. USA*, **100**, 11589-11593.

Mellor, E.A., Maekawa, A., Austen, K.F. & Boyce, J.A. (2001) Cysteinyl leukotriene receptor 1 is also a pyrimidinergic receptor and is expressed by human mast cells. *Proc. Natl. Acad. Sci. USA*, **98**, 7964-7969.

Nagata, M., Saito, K., Tsuchiya, K. & Sakamoto, Y. (2002) Leukotriene D4 upregulates eosinophil adhesion via the cysteinyl leukotriene 1 receptor. *J. Allergy Clin. Immunol.*, **109**, 676-680.

Ono, M., Yuasa, T., Ra, C. & Takai, T. (1999) Stimulatory function of paired immunoglobulin-like receptor-A in mast cell line by associating with subunits common to Fc receptors. *J. Biol. Chem.*, **274**, 30288-30296.

Paruchuri, S., Jiang, Y., Feng, C., Francis, S.A., Plutzky, J. & Boyce, J.A. (2008) Leukotriene E4 activates peroxisome proliferator-activated receptor gamma and induces prostaglandin D2 generation by human mast cells. *J. Biol. Chem.*, **283**, 16477-16487.

Pedersen, K.E., Bochner, B.S. & Undem, B.J. (1997) Cysteinyl leukotrienes induce P-selectin expression in human endothelial cells via a non-CysLT1 receptor-mediated mechanism. *J. Pharmacol. Exp. Ther.*, **281**, 655-662.

Ramires, R., Caiaffa, M.F., Tursi, A., Haeggstrom, J.Z. & Macchia, L. (2004) Novel inhibitory effect on 5-lipoxygenase activity by the anti-asthma drug montelukast. *Biochem. Biophys. Res. Commun.*, **324**, 815-821.

Spada, C.S., Nieves, A.L., Krauss, A.H. & Woodward, D.F. (1994) Comparison of leukotriene B4 and D4 effects on human eosinophil and neutrophil motility in vitro. *J. Leukoc. Biol.*, **55**,

183-191.
Vannella, K.M., McMillan, T.R., Charbeneau, R.P., Wilke, C.A., Thomas, P.E., Toews, G.B., Peters-Golden, M. & Moore, B.B. (2007) Cysteinyl leukotrienes are autocrine and paracrine regulators of fibrocyte function. *J. Immunol.*, **179**, 7883-7890.

Journal of Electron Microscopy Advance Access published November 11, 2009

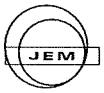

Journal of Electron Microscopy: 1–10 (2009)
doi: 10.1093/jmicro/dfp056

Physical: Full-length—Experimental

Morphological study of acoustic liposomes using transmission electron microscopy

Tetsuya Kodama[1,*], Noriko Tomita[1,5], Sachiko Horie[1], Nicolas Sax[1], Hiroko Iwasaki[1], Ryo Suzuki[2], Kazuo Maruyama[2], Shiro Mori[3] and Fukumoto Manabu[4]

[1]Graduate School of Biomedical Engineering, Tohoku University, 2-1 Seiryo, Aoba, Sendai, 980-8575, Japan, [2]Department of Biopharmaceutics, School of Pharmaceutical Sciences, Teikyo University, 1091-1 Suwarashi, Sagamiko, Sagamihra, Kanagawa, 229-0195, Japan, [3]Department of Oral Health Science, Tohoku University Hospital, 1-1 Seiryo, Aoba, Sendai, 980-8574, Japan and [4]Institute of Development, Aging and Cancer, Tohoku University, 4-1 Seiryo, Aoba, Sendai, 980-8575, Japan
[5]Present address: Institute of Fluid Science, Tohoku University, 2-1-1 Katahira, Aoba, Sendai, 980-8577, Japan
*To whom correspondence should be addressed. E-mail: kodama@bme.tohoku.ac.jp

Abstract Sonoporation is achieved by ultrasound-mediated destruction of ultrasound contrast agents (UCA) microbubbles. For this, UCAs must be tissue specific and have good echogenicity and also function as drug carriers. Previous studies have developed acoustic liposomes (ALs), liposomes that encapsulate phosphate buffer solution and perfluoropropane (C_3F_8) gas and function as both UCAs and drug carriers. Few studies have examined the co-existence of gas and liquid in ALs. This study aims to elucidate AL structure using TEM. The size, zeta potential and structure of ALs were compared with those of two other UCAs, human albumin shell bubbles (ABs; Optison) and lipid bubbles (LBs). ABs and LBs encapsulate the C_3F_8 gas. Particle size was measured by dynamic light scattering. The zeta potential was determined by the Smoluchowski equation. UCA structure was investigated by TEM. ALs were ~200 nm in size, smaller than LBs and ABs. ALs and LBs had almost neutral zeta potentials whereas AB values were strongly negative. The negative or double staining TEM images revealed that ~20% of ALs contained both liquid and gas, while ~80% contained liquid alone (i.e. nonacoustic). Negative staining AB images indicated electron beam scattering near the shell surface, and albumin was detected in filament form. These findings suggest that AL is capable of carrying drugs and high-molecular-weight, low-solubility gases.

Keywords nanobubbles, drug delivery system, sonoporation, ultrasound contrast agent, cavitation

Received 25 June 2009, accepted 5 October 2009

Introduction

Ultrasound contrast agents (UCAs) are nano/microbubbles that contain air or a high-molecular-weight, low water-solubility gas (e.g. C_3F_8, C_4F_{10} and SF_6) encapsulated in a lipid or albumin shell [1–6]. The diameters of UCAs vary from 100 nm to 10 μm and their behavior primarily depends on the ultrasound characteristics. The behavior of UCAs is described by an equation of motion that consists of external force, viscosity and stiffness terms [7]. When the external force is small, i.e. ultrasound pressure is small, UCAs undergo small volumetric oscillation (linear). With increasing ultrasound pressures, the amplitude of volumetric oscillation increases and

oscillation becomes aperiodic (nonlinear), resulting in destruction of UCAs [1,8].

Drug delivery via sonoporation using ultrasound and UCAs is a technique used for diagnosis and treatment [1,8] and is based on bubble destruction modes. During sonoporation, primary UCAs and subsequent bubble cavitation generated by the collapse of the UCAs induce mechanical forces such as liquid jets and shock waves [8]. These forces interact with the surrounding cells, resulting in the permeation of exogenous molecules into cells [1,8]. Sonoporation is a noninvasive, nonimmunogenic and tissue-specific procedure that has been used to treat cancer and many other diseases [1,3,9]. However, the efficiency of molecular delivery is relatively low; therefore, it has not been recognized as a clinically valuable approach. One strategy towards improving the efficiency of molecular delivery is to develop UCAs that are tissue-specific and that can function as drug carriers. Suzuki *et al.* [9] developed a novel form of liposome containing the C_3F_8 gas and phosphate buffer solution and demonstrated that it functions as an acoustic liposome (AL) applicable to a nonvirus molecular delivery system [5,6]. The liposome surface was covered with polyethyleneglycol (PEG); therefore, it was assumed that this molecule would not be incorporated by the reticuloendothelial system, thereby allowing a longer retention in the blood [10]. In addition, the tumor-targeting potential and drug-carrying capability are significantly improved by conjugating PEG with ligands specific for the target tissue and by producing bubbles with diameters of <100 nm, which allows for enhanced permeability and retention (EPR) effects [11,12]. These studies concluded that the liposome would be acoustic due to the differences between ultrasound backscatter intensities in the presence/absence of ultrasound. However, the coexistence of gas and liquid in the liposome has not been examined, neither have its size and structure been discussed.

The present study investigated the size, zeta potential and structure of ALs and compared these values with those of two other types of UCAs: a single human albumin shell (ABs; Optison) and lipid bubbles (LBs). Both UCAs encapsulated the C_3F_8 gas, which was identical to the liposome gas. Transmission electron microscopy (TEM) was used to assess the structure of UCAs, and the TEM images were obtained using either negative or double staining. The TEM findings will be used as parameters to evaluate biodistribution, safety and efficacy of micro/nanoparticulate systems.

Methods

Nano/microbubble preparation

Three types of UCA—ABs ($5.0–8.0 \times 10^8$ bubbles mL^{-1}; Optison™, Amersham Health Plc, Oslo, Norway), LBs and ALs—were used. LBs were created in an aqueous dispersion of 2 mg mL^{-1} 1,2-distearoyl-sn-glycero-phosphatidylcholine (DSPC) (Avanti Polar Lipids, Alabaster, AL, USA) and 1 mg mL^{-1} polyethylene glycol (PEG) distearate (Sigma-Aldrich) using a 20 kHz stick sonicator (130 W, Vibra Cell, Sonics & Materials Inc., Danbury, CT, USA) at 50% amplifying strength for 1 min, in the presence of C_3F_8 gas in a sterilized 7 mL Bijou vial [8,13,14]. The vial cap has two openings that serve as a gas inlet and outlet. During sonication, the C_3F_8 gas was kept under the condition of inflow and outflow through the openings. The LB concentration was 3.4×10^8 bubbles mL^{-1} [13]. ALs were prepared by modifying the protocol of Suzuki *et al.* [9]. First, DSPC (NOF Co., Tokyo, Japan) and 1,2-distearoyl-sn-glycero-3-phosphatidyl-ethanolamine-methoxy-polyethyleneglycol (DSPE-PEG2000-OMe) (NOF Co.) (94:6 [mol/mol]) were dissolved in 10 mL of 9:1 (v/v) chloroform/methanol. Next, 5 mL of phosphate-buffered saline (PBS) without Mg^{2+} and Ca^{2+} (pH 7.2 at room temperature, Sigma) was added to the solution. The solution was then sonicated using a 20 kHz stick sonicator (Sonics & Materials). Liposomes were obtained by reverse phase evaporation at 65°C. The organic solvent was completely removed, and the size of the liposomes was adjusted to <100 nm using extruding equipment (Northern Lipids Inc., Vancouver, BC, Canada) with three sizing filters (pore sizes: 100, 200 and 600 nm) (Nuclepore Track-Etch Membrane, Whatman plc, UK). The resulting liposomes were passed through a 0.45 μm pore size filter (MILLEX HV filter unit, Durapore polyvinylidine-difluoride (PVDF) membrane, Millipore Corporation, MA, USA) for sterilization. Lipid concentration was measured using the Phospholipid *C*-test Wako (Wako Pure Chemical Industries, Ltd, Osaka, Japan). To produce AL, a

liposome suspension of 1 mL (lipid concentration: 1 mg mL^{-1}) was sonicated using a bath sonicator (42 kHz, 100 W; Bransonic 2510J-DTH, Branson Ultrasounics Co., Danbury, CT, USA) and a 20 kHz stick sonicator (130 W, Sonics & Materials, Inc.) at 50% amplifying strength for 1 min, in the presence of C_3F_8 in a sterilized 7 mL Bijou vial, as described above.

Dark field microscopy

Immediately after sonication, 20 μL drops of either AL or LB were put on a glass cover and were observed under an inverted microscope (IX81, Olympus, Tokyo, Japan) equipped with an illuminator (Darlkite Illuminator, Micro Video Instruments, Avon, MA , USA).

Echogenicity measurement

The air inside the 5 mL vials containing 1 mL of liposome suspension (lipid concentration: 1 mg mL^{-1}) sealed with a rubber cap together with an aluminium jacket was replaced with 12 mL of air or C_3F_8 gas and supercharged with another 12 mL of each gas. The suspension in the vial was sonicated in a bath sonicator (Branson Ultrasounics) for 2 min. The suspension was transferred to a 7 mL Bijou vial and further sonicated by a 20 kHz sonicator (Sonics & Materials) at 50% amplifying strength for 1 min while 5 mL of each gas was injected at a rate of 300 mL h^{-1} using a syringe pump (model KDS 100, KD Scientific, Hollliston, MA, USA). Four milliliters of a 40-fold dilution with PBS were added to a well of a 6-well plate and the B-mode image was acquired with a high-frequency ultrasound imaging system with a center frequency of 55 MHz (VEVO 770, Visualsonics Inc., Toronto, Canada). The grayscale histogram of a selected ROI was measured using the implemented software of the US imaging system. The ROI circle was set to 1.00 mm^2, 1 mm above the bottom of the well.

Size and zeta potential

The size and zeta potentials of the bubbles were measured using a zeta potential & particle size analyzer (zeta potential range: −200 to +200 mV, particle size/distribution range: 0.6 nm to 7 μm, laser source: laser diode (660 nm), ELSZ-2, Otsuka Electronics, Osaka, Japan). The size was measured using the dynamic light scattering. The zeta potential was automatically calculated on the basis of the electrophoretic mobility using the Smoluchowski equation: $\zeta = 4\pi\eta u/\varepsilon$, where ζ is the zeta potential, u is the electrophoretic mobility and η and ε are the viscosity and dielectric constant of the solvent, respectively. The Smoluchowski equation is applicable to a solid surface on which a surface-charge layer exits and electrolyte ions do not penetrate through the surface, i.e. hard particles [15]. In the present study, the three types of bubbles were assumed to be hard particles. The bubble solutions were diluted in PBS to $\sim 10^7$ bubbles mL^{-1} at room temperature (21–23°C). The average values of the sizes and zeta potentials were calculated using four to nine independent measurements on each sample.

TEM

Either negative or double staining was used for AL. Negative staining was used for LB and AB. The stained samples were examined with a JEM-2000EX operated at 100 kV (JEOL Datum, Tokyo, Japan) at the Hanaichi UltraStructure Research Institute, Aichi, Japan; or with a H-7600 operated at 80 kV (Hitachi Tokyo, Japan) at Tohoku University, Sendai, Japan. For the negative staining, a 400-mesh grid (EM fine-grid F-400, Nisshin EM Co., Tokyo, Japan) with a carbon support film (10–20 nm in thickness) was used, and was given a hydrophilic treatment. Samples were stained at either room temperature or at 80°C. For the former case, a drop of sample solution, distilled water and phosphotungstic acid (Merck, Tokyo, Japan) were put on a parafilm (Pechiney Plastic Packaging Co., Menasha, WI, USA). The grid was put into the sample drop (30 s), then in a distilled water drop for washing (10 s) and finally in a phosphotungstic acid drop for staining (10 s). Any excess solution was removed with filter paper. For the latter case, a parafilm was floated on water heated at 80 °C, and the procedure outlined above was then followed. For the double staining, an AL solution generated in the presence of C_3F_8 in a sterilized 7 mL vial was immediately added to 1 mL of 2% agarose (Cambrex Bio Science Rockland, Inc., Rockland, USA) to obtain a stable solution that did not release gas. Then, the AL solution was mixed with the same amount of